JMEPEG (2024) 33:5061–5074
https://doi.org/10.1007/s11665-023-08292-8

1059-9495/$19.00

TECHNICAL ARTICLE

3D-Printed Sandwiched Acrylonitrile Butadiene Styrene/Carbon Fiber Composites: Investigating Mechanical, Morphological, and Fractural Properties

Rashi Tyagi, Gurminder Singh, Ranvijay Kumar, Vinay Kumar, and Sunpreet Singh

Submitted: 24 January 2023 / Revised: 4 April 2023 / Accepted: 29 April 2023 / Published online: 22 May 2023

3D printing of carbon fiber (CF)-reinforced thermoplastics has been reported for manufacturing economical consumer products. But hitherto, very little has been reported on 3D-printed hybrid composite structures prepared by sandwiching CF in the layer-by-layer manufactured functional prototype. The present work reports the 3D printing of CF sandwiched acrylonitrile butadiene styrene (ABS) (by varying the CF layers from 1 to 3) composite structure. The 3D printing parameters like the number of CF layers, the orientation angle of layers, and the printing temperature of the nozzle were designed by Taguchi L_9 orthogonal array. The mechanical properties obtained (ultimate tensile strength (UTS): 58.51 MPa, modulus of toughness (MT): 1.566 MPa, and Young's modulus (E): 1009.994 MPa) were optimized to ascertain the acceptable strength of functional parts for commercial 3D printing applications. The parametric optimization highlighted that the acceptable orientation angle of CF in ABS matrix is 0°. Along with 03 numbers of CF layers and 250 °C printing nozzle temperature, functional parts with acceptable mechanical properties may be fabricated. The morphological analysis of the fractured surface outlined that the 3 layers of CF correspond to acceptable mechanical properties in the 3D-printed functional prototype. The mechanical and morphological results are supported by x-ray diffraction (XRD) and Fourier transform infrared (FTIR) spectrometric analysis.

Keywords 3D printing, acrylonitrile butadiene styrene, carbon fibers, EDS, FTIR, mechanical analysis, morphological analysis, parametric optimization, SEM, XRD

1. Introduction

Lightweight sandwich structures have attracted researchers' attention for their numerous applications in various industrial sectors, such as aerospace, building, marine, windmill, and automobile (Ref 1-4). The excellent properties of sandwich structures consist of high flexural stiffness, high energy absorption abilities, and thermal insulation. Sandwich structures are mainly comprised of two solid skins at the top and bottom, which are connected by a lightweight core to provide a high buckling and bending resistance (Ref 5-7). A lightweight core also provides shear stiffness, while the top and bottom skins provide high tensile and compressive strength; in the case of conventional manufacturing processes, it is noticed that a costly and complicated bonding process is involved. Consequently, simple technology is required to facilitate the formation of the skins and intricate-shaped core in a single piece. Also, a complete examination of the functional properties must be done as obtained from a core shape and verification of these properties that suit the desired application. Hence, technology is desirable to facilitate both flexible design and fabrication of core shapes (Ref 8, 9). Recent innovations in additive manufacturing offer the capability to manufacture the architected cellular cores of free-form 2D and 3D topologies, which cannot be easily produced by other processes (extrusion, expansion, and corrugation). Among all these AM technologies, laser sintering (SLS) and fused filament fabrication (FFF) are the most attractive 3D printing technologies to process polymer composites. Compared to SLS, the FFF technique exhibits the benefits of negligible wastage, low input energy, less material cost, and a consistently precise prototype (Ref 10-13). Further, other advantages of FFF are that there is no requirement in chemical post-processing and cost-effective materials, which makes it economical. However, parts fabricated by FFF have inadequate mechanical characteristics (Ref 14-16). The limitations can be overcome by introducing new methods to prepare 3D-printed composites, such as various short-fiber-reinforced composites and particle-reinforced composites.

CF-reinforced plastic composites have several attractive properties, due to which they are rapidly used nowadays for many applications. FFF has been reported to be one of the AM processes for manufacturing CF-reinforced plastic composites. While applying CF as a reinforcement in the FFF process, a

Rashi Tyagi and **Ranvijay Kumar**, University Center for Research and Development, Chandigarh University, Mohali 140413, India; and Department of Mechanical Engineering, Chandigarh University, Mohali 140413, India; **Gurminder Singh**, Department of Mechanical Engineering, Indian Institute of Technology Bombay, Mumbai 400076, India; **Vinay Kumar**, University Center for Research and Development, Chandigarh University, Mohali 140413, India; and **Sunpreet Singh**, Department of Mechanical Engineering, National University of Singapore, Singapore 11570, Singapore. Contact e-mails: gurmindersingh2012@gmail.com and Gurminder.singh@iitb.ac.in.

proper investigation of the process parameters should be done to achieve a high-quality CF-reinforced composite. Besides the process parameters, composite parts fabricated by 3D printing are also influenced by the fiber orientation incorporated into the polymer matrix, infill density, infill patterns, and the number of fiber layers and their arrangement (Ref 17-20). A series of research has been reported in this direction, such as preparing composite filaments with the help of ABS extrusion at various contents of chopped CF. It has been reported that the tensile strength of prepared specimen with short CF at 5 wt.% and 150 μm length was enhanced by 22.5% than that of pure ABS specimen (Ref 14). Some studies have been reported on chopped glass fibers into ABS by FFF printing to improve tensile strength. They reported an increase in interlayer bond strength with increased contents of fiber due to fibers bridging' along with the layers (Ref 20-22). Further, CF-reinforced thermoplastic composite samples with the help of Markforged to attain details related to the mechanical properties of fiber filament. They prepared tensile samples, and a ninefold improvement in strength was found. In this work, the cutting of the test specimen was performed post-printing to eliminate extra matrix material and 'discontinuities'' that might affect the strength (Ref 23). FFF of short-fiber-reinforced filament of nylon with the help of a standard MarkOne 3D printer was used to print a composite specimen of CF and Nylon. They showed tensile strength comes out to be more than that of short-fiber-reinforced nylon printed parts (Ref 18, 24). However, a limited range of investigations has been reported on the influence of FFF printing parameters (temperature, fiber orientation, number of fiber layers, and infill density) on the mechanical behavior of fiber-reinforced composite. In this investigation, CF-reinforced tensile specimen is fabricated with the help of FFF-based 3D printer. Further, the tensile properties are obtained by conducting the tensile testing. Moreover, the fracture interfaces of specimens after the tensile test are reported by an SEM to elaborate material failure mode.

2. Materials and Method

Acrylonitrile butadiene styrene (ABS) is used as a matrix material. In this study, CF is selected as reinforcement due to its high specific stiffness, high specific strength, and high heat resistance, which causes the high temperature at the extruder. Figure 1 shows the FESEM and EDS of CF. Microscopic images show that the surface of CF is smooth and does not exhibit grooves, which can ensure good mechanical properties. The purity of fiber is confirmed by EDS, which shows that the carbon atom percentage is 100%. Table 1 specifies the CF properties as per the manufacturer's technical data.

XRD images of CF are given in Fig. 2. The CFs are composed of both microcrystals and amorphous carbons. The crystalline form of CF is found with some amount of an amorphous state. The fractions of the crystalline carbon and the amorphous carbon nanoclusters were calculated as per the reported literature (Ref 8).

2.1 3D Printing of Sandwich Structure

A 3D printer/FDM unit (Model: Creality Ender 3 Pro, permissible printing size: 220 × 220 × 250 mm, maximum bed temperature ≤ 110 °C) was used to fabricate the composite sandwich structure. The layer height of 0.16 mm has been selected for the preparation of the sandwiched structures. ASTM D638 standard was followed to fabricate the tensile specimen in order obtain the tensile properties. The 3D CAD design is exported as an standard triangulation language (i.e., STL file) format. A creality software is used for slicing to obtain the G-code from this STL file. In this process, the sandwich-structured specimen was prepared when the chopped single CF layer was spread in the 0° direction over the 50% 3D-printed ABS surface, forming a bottom face skin. By injecting the acetone over the spread fiber, it is possible to glue/adhere them with the printed bottom of ABS. Then, the continuous printing process was performed under a line pattern.

Consequently, the top skin, bottom skin, and core get printed in a single piece. Finally, the same process is repeated after changing the orientation to 45° and 90° as per the number of layers inside the sandwich structure increased and varied from 1 to 3. The key printing parameters utilized in this work are designed based on Taguchi L_9 array and are given in Table 2. Further, a pure ABS tensile sample was printed without applying chopped CF in the core to compare its properties with the prepared sandwich structure.

2.2 Mechanical Characterization

The universal testing machine (Max load- 5kN; Make-Shanta Engineering, India) under a tensile load of 100 kN was utilized to attain the mechanical properties of tensile specimens. The specimens were loaded till the material failure at a 50 mm/min strain rate. Then, SEM and EDS analysis (Model-JSM IT500; Make-Jeol) was conducted to observe the fracture morphology of all the tested specimens. The fractured surface image capturing has been performed at 500 and 100 μm. Figure 3 shows the photograph showing the specimen's failure at the 'shoulder' area during the tensile test. The weight percentage and elemental investigations of fractured samples have been carried out by EDS analysis. Further, the captured images of the fracture area were uploaded in the surface profilometry Gwyddion 2.55 software. The cutoff length value of 0.04 mm has been selected to study the fractured surface. The phase analysis was conducted on D8 ADVANCE ECO (Make: Bruker Scientific Instruments, Massachusetts). Further, FTIR was performed for analysis of bonding characteristics.

3. Results and Discussions

3.1 Effect of Process Parameters on Tensile Properties

Tensile testing of the prepared samples resulted in the estimation of mechanical properties such as ultimate tensile strength (UTS), peak strain (PS), break Strain (BS), modulus of toughness (MT), fracture tensile strength (FTS), and Young's modulus (YM). The recorded outcomes and observations in response to L_9 Taguchi experimental approach (refer to Table 2) are indicated in Table 3 and signal-to-noise ratios (S/N) in Table 4. By considering a ''larger is better'' approach, the responses such as UTS, FTS, PS, BS, YT, and YM are optimized. Figure 4 presents the S/N ratio plots for the obtained responses/output to evaluate the influence of various levels of I/P parameters, which will help obtain the optimized I/P parameters at a specific O/P parameter. From Fig. 4(a-f), it can be observed that the angle of fiber deposition at the lower

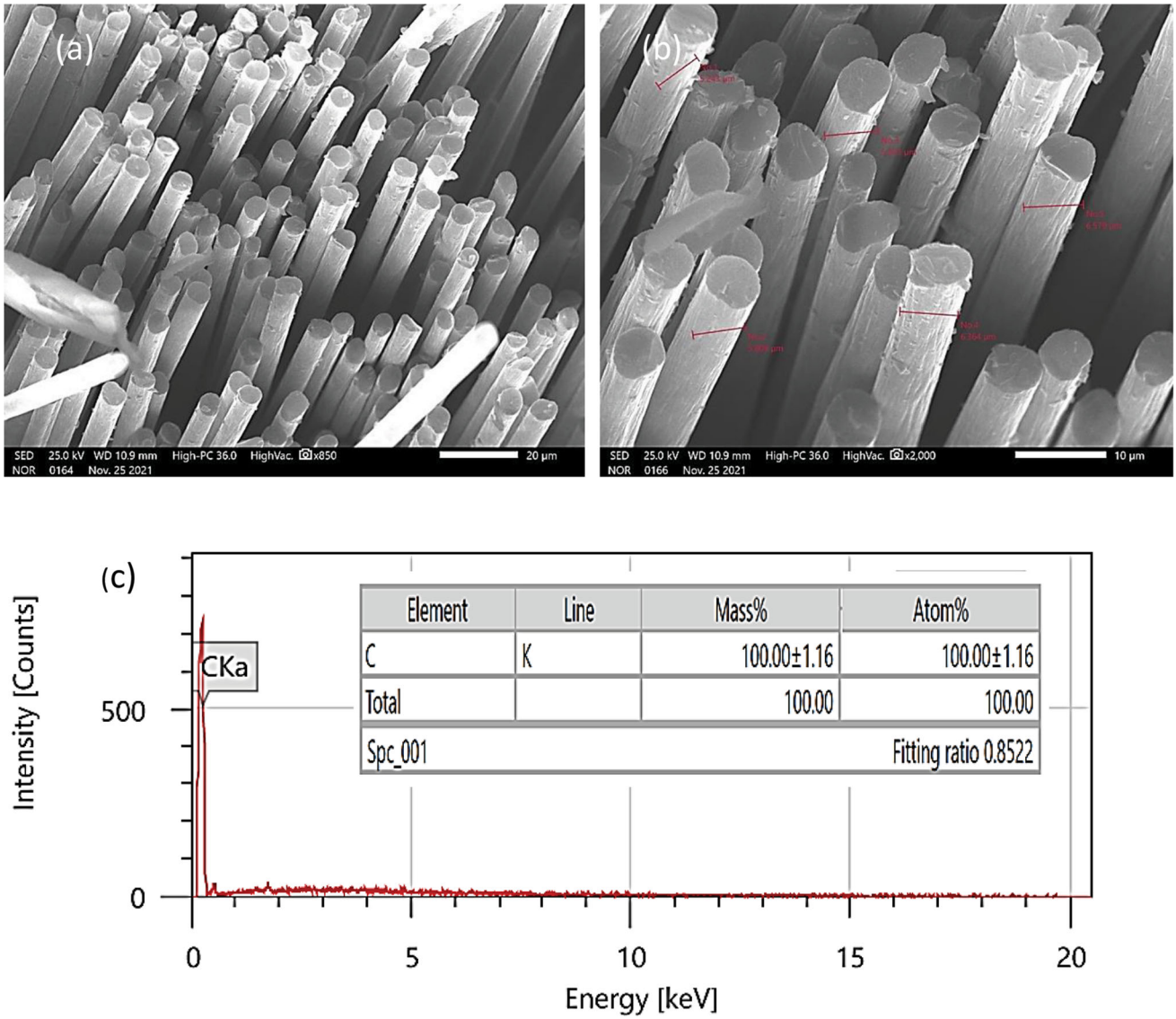

Fig. 1 (a), (b) SEM and (c) EDS of CFs

Table 1 Properties of the materials used

Properties	ABS	CF
Density	1.00–1.22 g/cm^3	1.79 g/cm^3
Ultimate tensile strength	33–110 MPa	4723–4482 MPa
Youngs Modulus	1.12–2.87GPa	231 GPa
Elongation at break, %	3–75%	1.7–1.8%
Glass transition temperature	105 °C	…
Strength to weight ratio	31–80 Pa-m^3/kg	…

level, nozzle temperature, and the number of fiber layers at the higher level result in maximum UTS, FTS, PS, BS, MT, and YM. Therefore, an optimum value of UTS, FTS, PS, BS, MT, and YM is achieved at the angle of fiber deposition at the lower level, nozzle temperature, and the number of fiber layers at a higher level.

The stress–strain curves were obtained for all the prepared 9 specimens of ABS-C and pure ABS specimens subjected to the tensile testing. Figure 5 and 6 shows the tensile strain–stress curves for pure ABS and ABS-C specimens with different experimental settings, respectively. Effects of nozzle temperature, number of fiber layer, and orientation of fiber on tensile properties (including UTM, FTS, PS, BS, YE, and toughness) of fiber-reinforced composite specimens are shown in Fig. 6. As shown in Fig. 5, for ABS, the stress–strain curves initially follow Hooke's law (stress is proportional to strain) till the ultimate yield point corresponds to the strain. After this point, little necking started and continued till the occurrence of fracture by showing no strain hardening. By sandwiching CFs within pure ABS, the tensile and fracture strength increased over pure ABS under different parameters. The tensile strength increased when the two fiber layers overlapped at each edge along the direction of tensile force. The breaking point generally falls at the edges as it is subjected to maximum tensile force. However, during printing, the fibers may have slipped from the matrix, particularly in the corner area resulting in limited fiber connection among the bottom edges and core, resulting in defects in prepared structure (Ref 25).

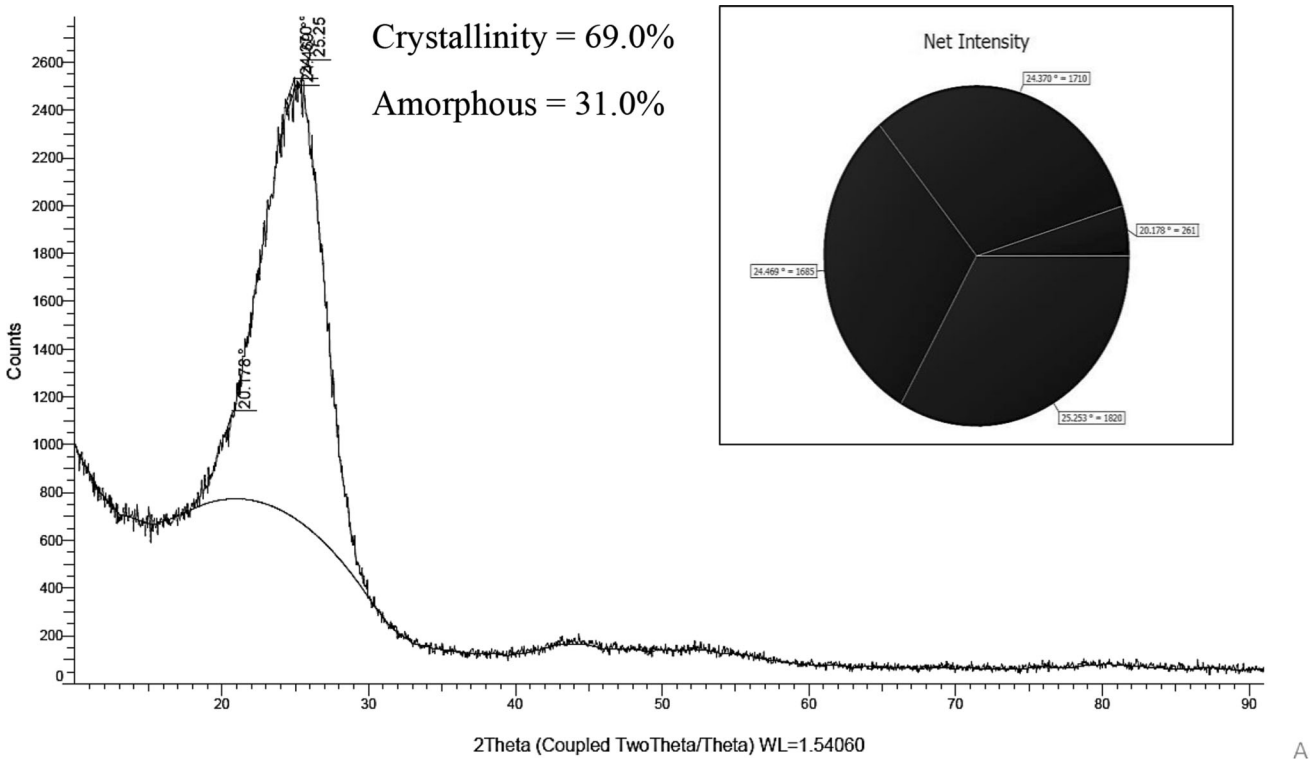

Fig. 2 XRD of CFs

Table 2 Experimentation settings based on Taguchi L_9 orthogonal array

Sr. No	No. of layers	Angle of fiber deposition, °	Nozzle temperature, °C
1	1	0	230
2	1	45	240
3	1	90	250
4	2	0	240
5	2	45	250
6	2	90	230
7	3	0	250
8	3	45	230
9	3	90	240

For UTS and YM, the optimum value has been obtained at 3 layers of fiber, 0° angle of deposition, and 250 °C of nozzle temperature. Figure 6(a) illustrates that with increasing number of CF layers from 1 to 3 and reducing the angle of deposition from 90° to 0°, tensile strength increased. The largest mean value (58.51 MPa) of UTS was observed at a 0° angle of deposition and 3 fiber layers, whereas the smallest value of mean was 31.63 MPa when the fiber layer was set at 1 (almost like pure ABS). Also, the FTS of the developed sandwich composite increased from 30.65 to 52.65 MPa with an increase in fiber layer from 1 to 3. This may be because with the rise in the fiber layer within the composite, the resistivity of the composite sandwich structure against FTS increased. In the case of nozzle temperature, it is found that the FTS of the composite increased with the temperature to 250 °C. This is because the higher nozzle temperature required fusion between fiber layers, resulting in the most resistive combination for bending deformation. Moreover, the deposition angle is a significant factor in influencing the mechanical properties. Moreover, fiber-reinforced composites generally generate the maximum tensile strength when fiber distribution is parallel to the loading (longitudinal direction) when specimens have 0° fiber orientation (Ref 26). Inversely, the strength of the composite will get reduced by changing the orientation of the fiber to 90°. In the case of samples with longitudinal fiber direction, most of the resistance against loading takes place within shell layers due to load enduring capability of oriented fibers. Shorter fibers are more randomly oriented at 45° and 90°, while longer fibers with more contribution to strength are better oriented in the mold flow direction. The fiber has a short length when oriented in 45° and 90° directions than those in the 0° direction. As a result, specimens printed in 45° and 90° fiber directions indicate lower tensile strength, while the strength considerably increases in the 0° fiber direction.

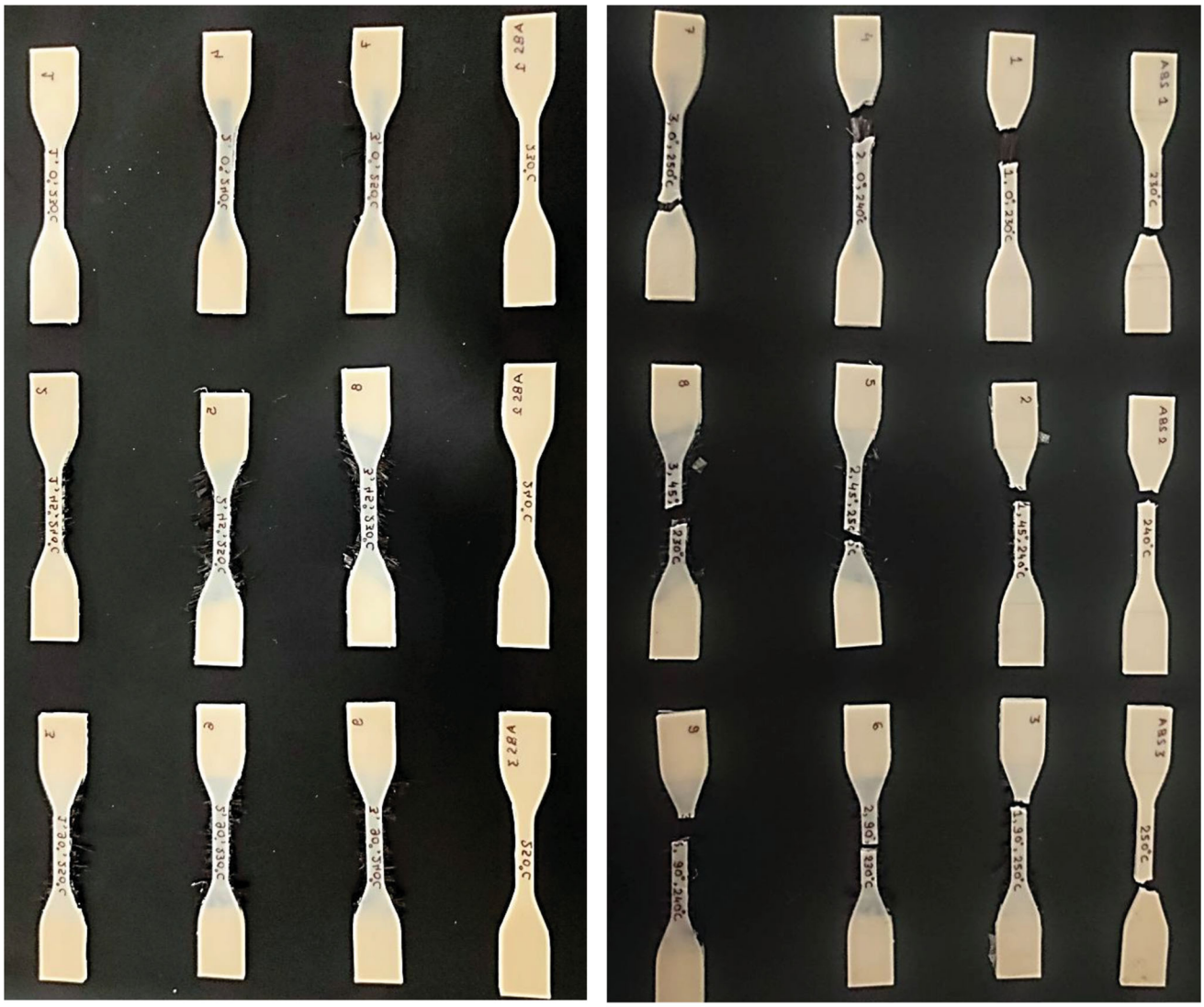

Fig. 3 Photograph showing the specimen's failure at the 'shoulder' area during the tensile test

Table 3 Observations for mechanical properties

Sample	UTS, MPa	FTS, MPa	PS	BS	MT, MPa	YM, MPa
1	39.65	37.18	0.050	0.049	0.910	782.211
2	35.96	32.36	0.050	0.049	0.792	709.415
3	31.63	30.27	0.036	0.035	0.529	873.590
4	42.10	40.29	0.058	0.042	0.846	713.976
5	41.25	38.10	0.043	0.045	0.866	949.404
6	32.43	29.19	0.050	0.049	0.715	639.775
7	58.51	52.65	0.057	0.059	1.566	1009.994
8	45.20	40.68	0.054	0.056	1.139	832.254
9	32.54	29.28	0.047	0.045	0.666	691.326
ABS (230 °C)	43.34	39.00	0.057	0.056	1.092	748.131
ABS (240 °C)	42.16	37.95	0.057	0.056	1.062	727.761
ABS (250 °C)	32.20	28.98	0.039	0.038	0.557	808.484

Table 4 Signal-to-noise ratios (S/N) for mechanical properties of sandwich composite

Sample	S/N ratio for UTM, dB	S/N ratio for FTS, dB	S/N ratio for PS, dB	S/N ratio for BS, dB	S/N ratio for MT, dB	S/N ratio for YM, dB
1	31.964	31.406	− 26.020	− 26.196	− 0.819	57.866
2	31.116	30.200	− 26.020	− 26.196	− 2.025	57.018
3	30.002	29.620	− 28.873	− 29.118	− 5.530	58.826
4	32.485	32.103	− 24.731	− 27.535	− 1.452	57.073
5	32.308	31.618	− 27.330	− 26.935	− 1.249	59.549
6	30.218	29.304	− 26.020	− 26.196	− 2.913	56.120
7	35.344	34.428	− 24.882	− 24.583	3.895	60.086
8	33.102	32.187	− 25.352	− 25.036	1.130	58.405
9	30.248	29.331	− 26.558	− 26.935	− 3.530	56.793

3.2 Optimization of Process Parameters

From the analysis of variance (ANOVA), as shown in Table 6, the loading of the fiber layer at a specific angle in ABS is significant to obtain high strength with a contribution of 63.29%. The number of fiber layer and extrusion temperature also have a significant effect, with a contribution of 22.98 and 10.43%. As shown in Table 6, the reason for best setting parameters for fiber deposition at 0°, nozzle temperature at 250°, and the number of fiber layers at 3 is that these settings have contributed to uniform deposition of fiber layers with significant compactness, higher structural strength, and controllable rate of heating within the ABS-C sandwich structure. The best input parameter as the angle of deposition is obvious because the 90° deposition angle of fiber will lead to sudden pulling and separation of fiber during the deformation. In contrast, a 0° deposition angle of fiber will provide better resistance to deformation. The behavior of the number of fiber layers, angle of deposition, and extrusion temperature was examined (Tables 5 and 6), which shows that the percentage contribution of the number of fiber layers and extrusion temperature is quite low compared to the angle of deposition. The residual error is found to be 3.29% which confirms the significant accuracy of the predicted model. This error value also highlights that no higher measurement error is there during the experimentation.

3.2.1 Optimization of Ultimate Tensile Strength (UTS). Taguchi design-based formula has been used for optimization which is:

$$\eta_{\text{opt}} = \text{M} + (\text{M}_{\text{A3}} - \text{M}) + (\text{M}_{\text{B1}} - \text{M}) + (\text{M}_{\text{C3}} - \text{M})$$

whereas 'M' = overall mean of S/N data, M_{A3}, M_{B1}, M_{C3} = Mean of S/N data with no of layers at level 1, angle of deposition at level 1, and extrusion temperature at level 3.

$$y^2_{\text{opt}} = (10)^{\eta\text{opt}/10} \qquad \text{(for properties, Larger is better)}$$

Here, overall mean (M) of S/N ratio was obtained by Minitab software.

$$\text{M} = 31.85$$

Then, S/N ratios obtained from response table are: $M_{\text{A3}=}32.90$, $M_{\text{B1}} = 33.21$, $M_{\text{C3}} = 32.55$.

Now, $\eta_{\text{opt}} = 31.85 + (32.90 - 31.85) + (33.21 - 31.85) + (32.55 - 31.85) = 34.96$ db

$$\text{So, } y^2_{\text{opt}} = (10)^{\eta\text{opt}/10}$$

$$y_{\text{opt}} = \sqrt{10^{35.02/10}} = 55.97 \text{ MPa}$$

The confirmatory experiment for UTS was carried out, and 58.51 MPa value was obtained which is near to the predicted value.

The above-given optimization study is also carried out for FTS, PS, BS, MT, and YM to verify the accuracy in experimental results. Then, the experimental and predicted values for each mechanical property have been calculated (Table 7).

3.3 Fracture Interface Morphological Analysis

A study on fracture morphology for all specimens was carried out to explore the mechanical behavior of an FFF printed sandwich. The reason for such mechanism and the fracture interface of ABS-C composite sandwich after tensile testing layers was studied with the help of SEM at varrying number of fiber in order to observe the defects in specimen along with the interfacial adhesion among thermoplastic matrix and fibers. Figure 7 shows the captured SEM images of fractured sample surface for sample 3 (1 fiber layer, 250° temperature, and 90° angle of deposition) and sample 7 (3 fiber layer, 250° temperature, and 0° angle of deposition) after tensile tests. In the case of a fiber-reinforced polymer, the interaction between matrix interfaces and fiber plays an important role in specimen performance. In one of the researches, the performance of the fiber-reinforced composite is reported which is proportional to properties of fiber–matrix interface (Ref 27). SEM micrographs in Fig. 7(a) for sample 3 with the one-carbon layer show that porosity is higher, resulting in the weakest ABS-C composite specimen. Figure 8(a1) for sample 7 with 3 carbon layers shows that the interlayer of fused deposition is strongly bonded and ABS as matrix material is infused within the fibrous bundles, thereby making the structure with excellent interfacial bonding to achieve high tensile properties. Figure 7(b) and (b1) illustrates the fiber pulling-out under tensile testing with a single fiber layer and three-carbon layer composite due to plastic deformation and brittle failure, respectively. These results are inline with previously reported studies that brittle failure of matrix and fracture of fiber occur along the longitudinal direction (Ref 21). On the other hand, plastic deformation of matrix occurs in a transverse direction close to the fiber ends within the core, whereas shell layer describes brittle failure of matrix and the mechanism of pulling out of fibers (Ref 28). This may be due to the higher porosity of the specimen with single CF, which also had the lowest tensile

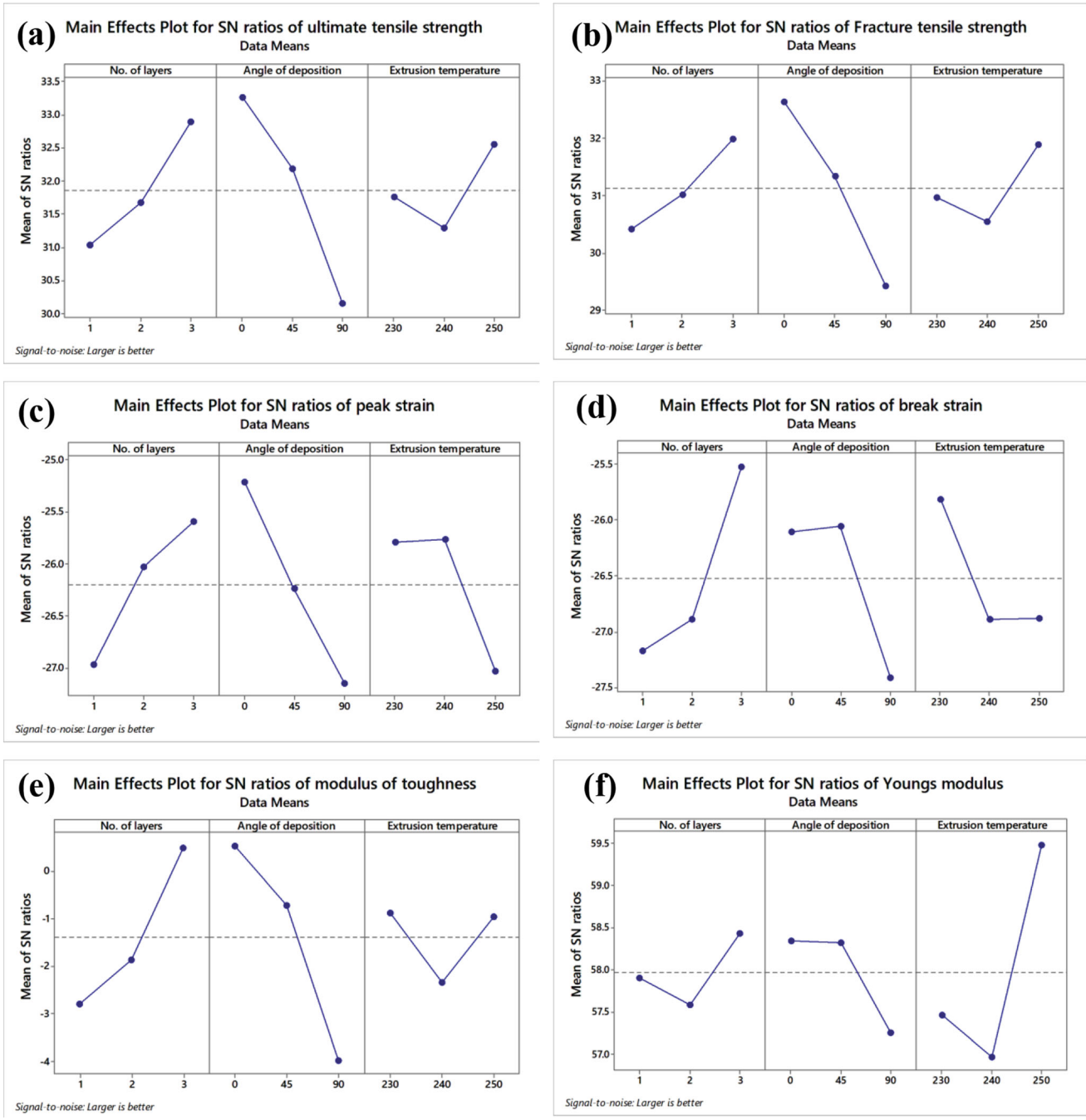

Fig. 4 S/N ratios plot for: (a) TS (b) FS (c) PS (d) BS (e) MT (f) YM

properties. Figure 7(b1) showing SEM micrographs confirms that CFs are pulled out of the matrix for 1 fiber layer, pointing toward the failure of interfacial bonding between CFs and thermoplastic matrix to provide the required reinforcement within the composites. Specimens with a single layer of fiber also had relatively lesser ultimate tensile strength (Fig. 6). Fiber orientation always affects the composite properties. The strength of longitudinally oriented composites is generally higher as compared to transversely oriented fiber composites (Ref 29). Similar observations have been reported by some other researchers as per reported literature (Ref 30-32). Therefore, sample 7 at 0° fiber deposition shows good tensile properties and confirms that this result in the fabricated composite is due to the effectiveness of CFs in strengthening the ABS-C composites.

EDS study of sample 3 (90° angle of fiber deposition) and sample 7 (0° angle of fiber deposition) was carried out to enquire the fraction of carbon and to conform its presence. Figure 8 illustrates the EDS analysis of sample 3 and sample 7. The mass fraction of CFs in sample 3 and sample 7 has been observed at 100%, which verifies that the CF is uniformly dispersed.

3.4 Surface Roughness

Figure 9 illustrates the 3D fracture morphology and surface profilometry of sample 3 and sample 7. Sample 3 showed

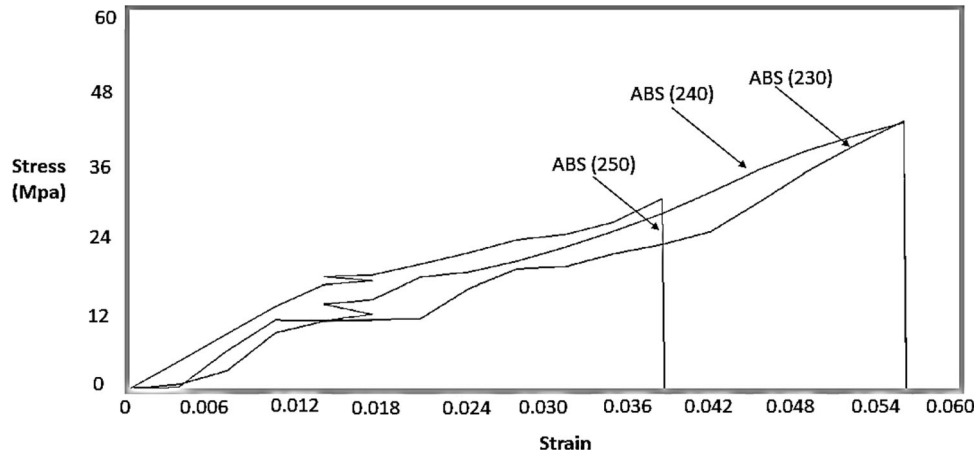

Fig. 5 Stress versus strain curve of tensile testing for pure ABS specimen

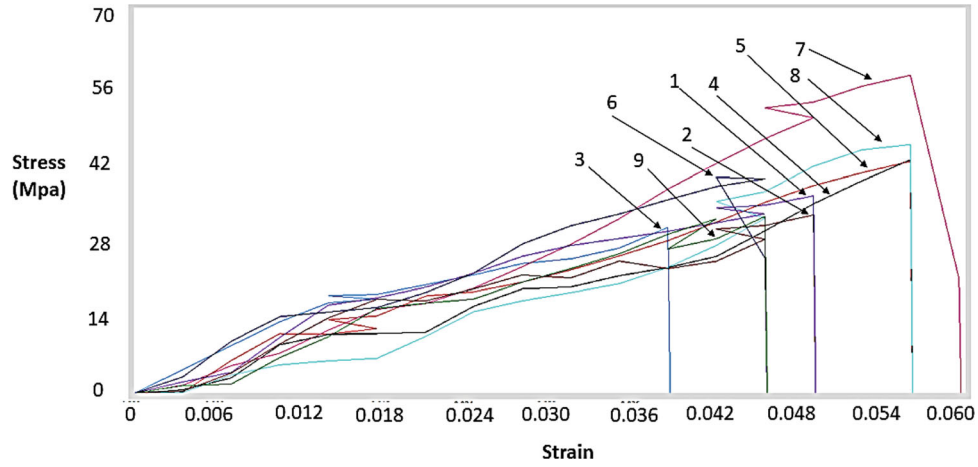

Fig. 6 Stress versus strain curve of tensile testing for ABS-C specimen

Table 5 Analysis of variance for S/N ratios

Source	DF	Seq SS	Adj SS	Adj MS	F	P	Percentage contribution
No. of layers	2	5.4207	5.4207	2.7103	6.98	0.125	22.98%
Angle of deposition	2	14.9279	14.9279	7.4640	19.23	0.049	63.29
Extrusion temperature	2	2.4609	2.4609	1.2304	3.17	0.240	10.43
Residual error	2	0.7764	0.7764	0.3882			3.29
Total	8	23.5859					

Table 6 Response table for signal-to-noise ratios larger is better for ultimate tensile strength

Level	No. of layers	Angle of deposition	Extrusion temperature
1	31.03	33.27	31.76
2	31.67	32.18	31.28
3	32.90	30.16	32.55
Delta	1.87	3.11	1.27
Rank	2	1	3

higher surface roughness than sample 7 (Ra = 178.2 μm) because of the fracture mode of sample 7 (Ra = 172.6 μm), which is brittle. The formation of pores may also be the reason of this higher surface roughness, whereas the approximate flat cross-sectional fracture of sample 7 leads to a low surface roughness value.

Table 7 Experimentally evaluated values and predicted value of mechanical properties

Sample	Attribute	Output parameters					
		UTS	FTS, Mpa	PS	BS	MT	YM, N
Extruded ABS-C Sample 7	η_{opt}, dB	34.96	34.26	− 24.2	− 25.35	2.94	60.32
	Predicted value, y_{opt}	55.97	51.64	0.061	0.054	1.4028	1037.52
	Actual value at optimized setup	58.51	52.65	0.057	0.059	1.566	1009.994

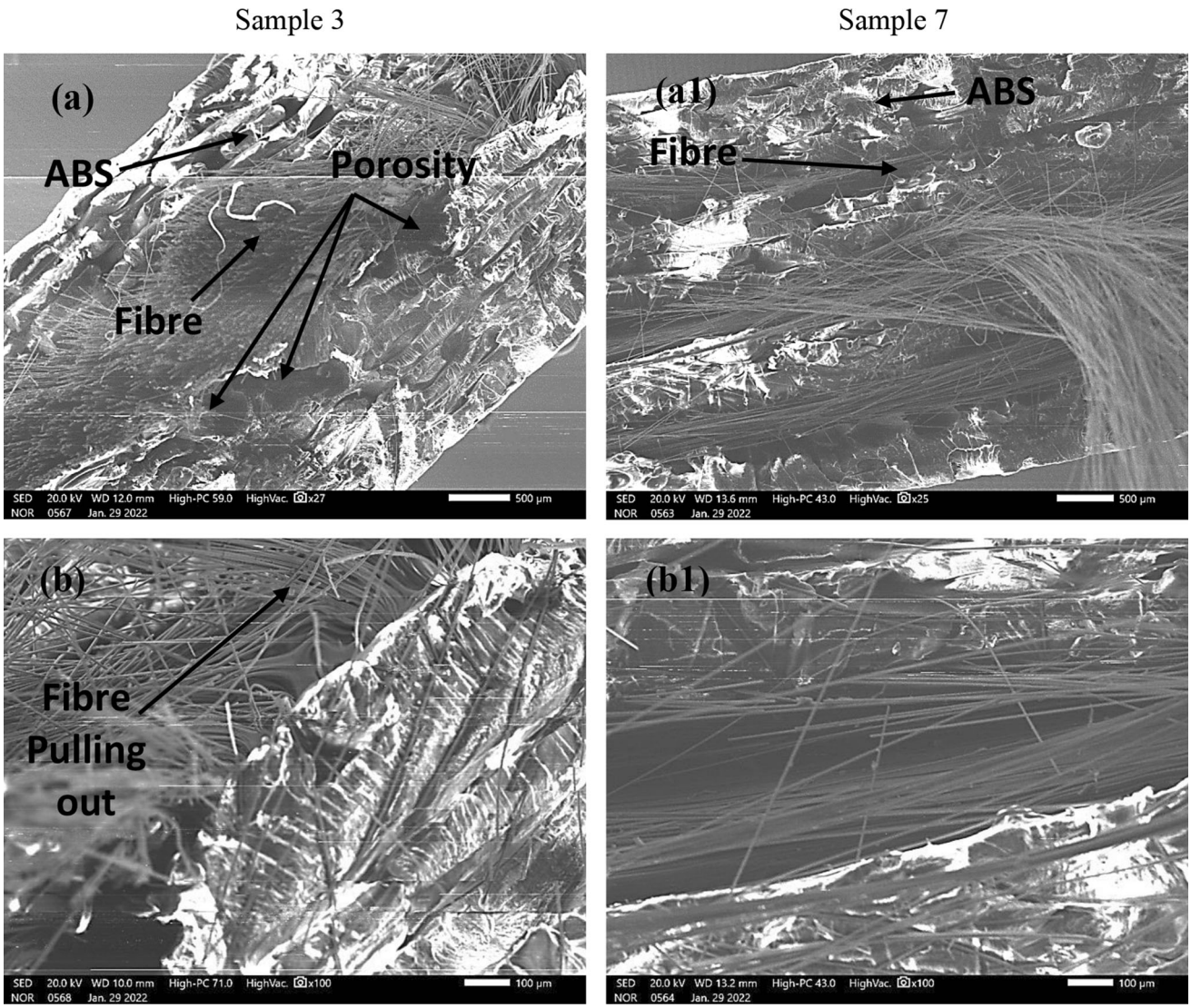

Fig. 7 SEM fracture interface of specimens with different CF contents after tensile testing

3.5 XRD Analysis

The XRD profile of ABS and ABS-CF composites is presented in Fig. 10. It was observed that ABS sample with no CF layer possesses low bond strength for 20° coupled with two theta wavelengths (WL) as compared to composite samples. The amorphous (67.9%) and crystallinity (32.1%) phase of ABS (shown in Table 8) was noticed. The addition of CF layers improved the amorphous phase of ABS for better bond characteristics and mechanical strength. The ABS-3 CF layer composite outlined acceptable amorphous (71.1%) and crystallinity (28.9%) phase (in which the CF deposition angle of 0° was considered) may result in good mechanical and morphological properties for the proposed engineering applications. The observations obtained for mechanical and morphological properties are inline with previous studies (Ref 17, 18). The results obtained in Table 8 for crystallinity and amorphous of the functional prototypes outlined that the addition of 3CF layers in ABS resulted in decrease in crystallinity of ABS from 32.1 to 28.9. This is because the amorphous nature of CF significantly contributed in increasing the conductivity of the ABS composite that resulted in decreased crystallinity and

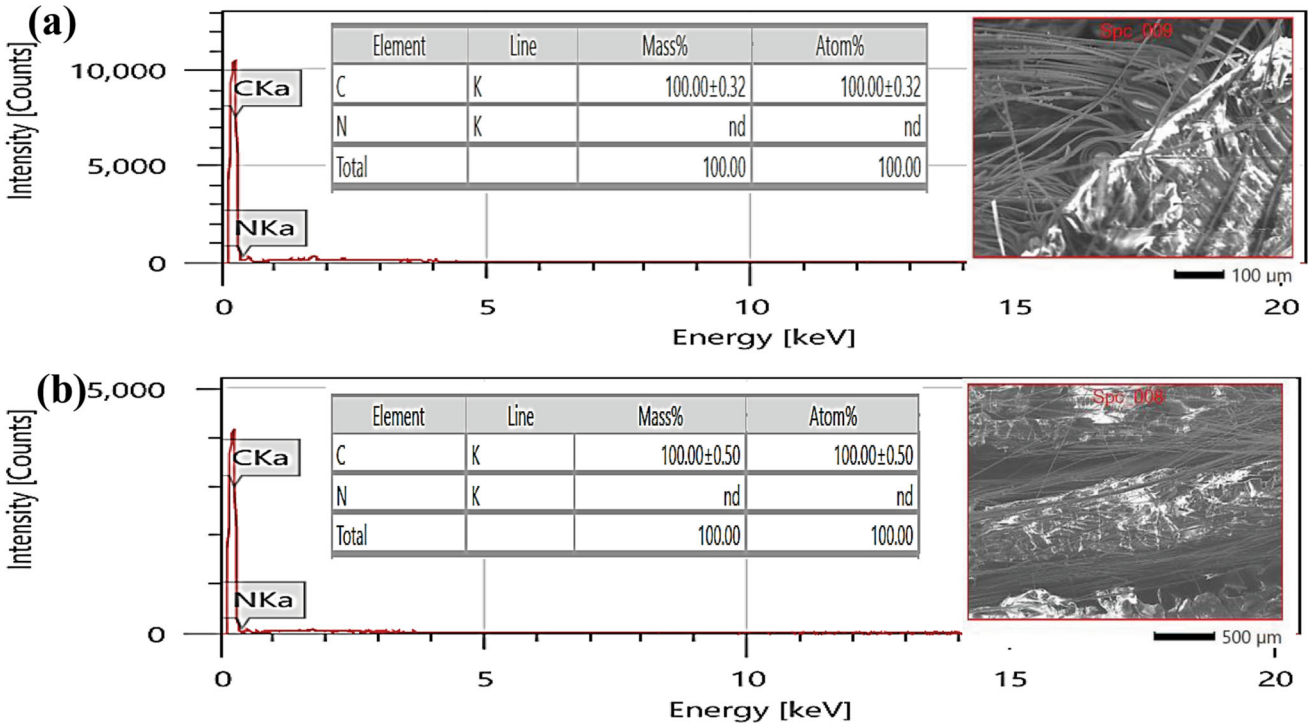

Fig. 8 EDS analysis conducted on (a) sample 3 and (b) sample 7

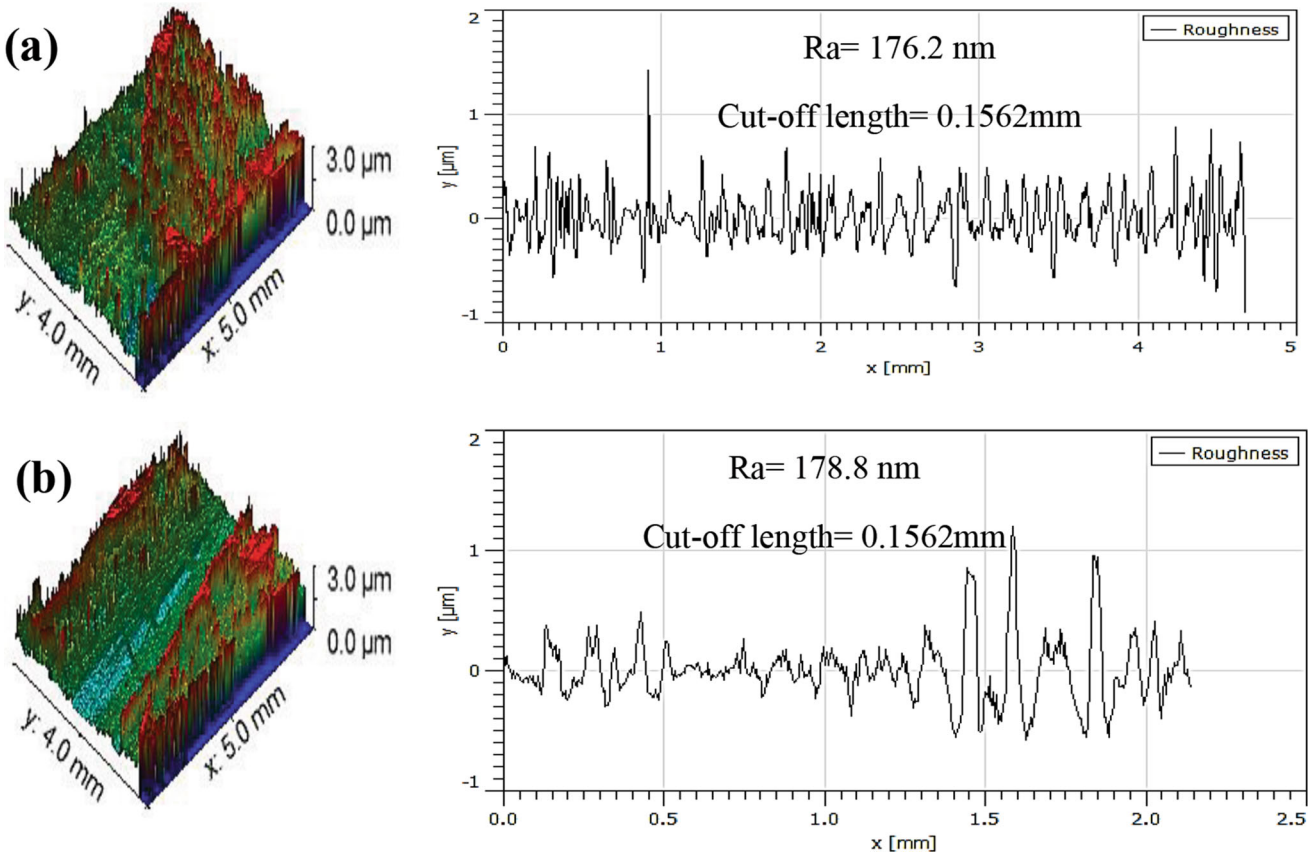

Fig. 9 3D fracture view and surface profilometry of (a) sample 7 and (b) sample 3

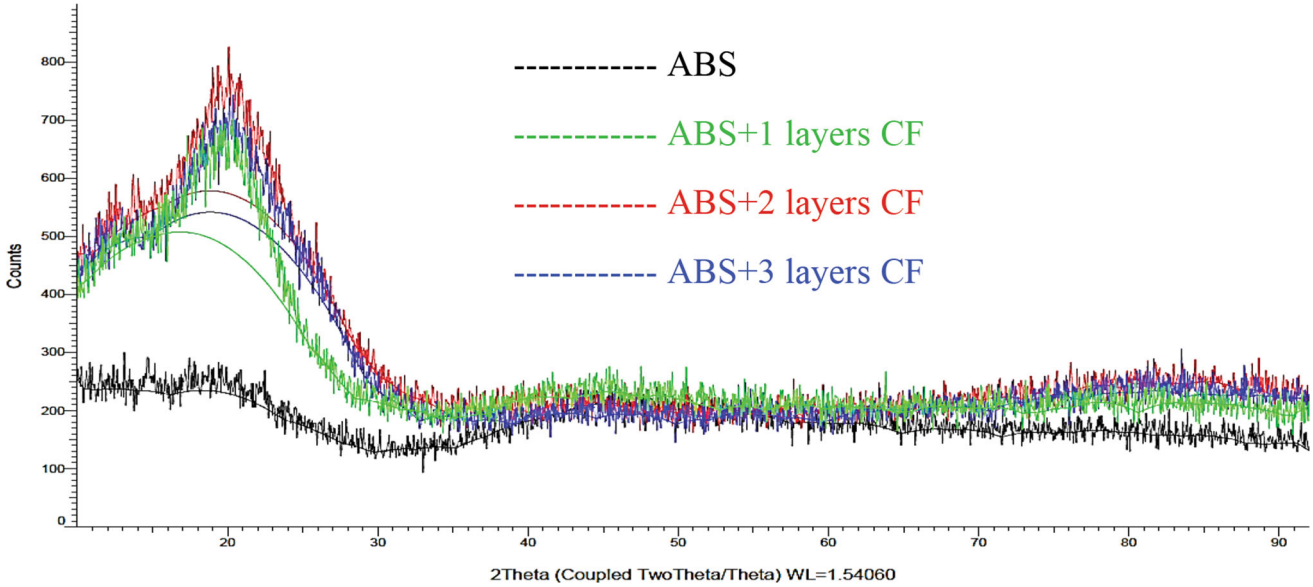

Fig. 10 XRD plots for ABS and ABS-CF samples

Table 8 Crystallinity% and amorphous% of ABS and ABS-CF composites

Sample	Amorphous, %	Crystallinity, %
ABS	67.9	32.1
ABS + 1 CF layers	72.9	27.1
ABS + 2 CF layers	71.4	28.6
ABS + 3 CF layers	71.1	28.9

hence increase in the amorphous phase (i.e., from 67.9 to 71.1) (Ref 21).

3.6 FTIR Analysis

ABS and ABS-CF composites were analyzed using FTIR to identify the presence of different chemical constituents and compare them with previously reported studies (Ref 26, 27). Figure 11 shows the absorbance spectrum of ABS samples (as per Table 8) obtained from the Analytical 3000B FTIR system (Make: Analytical Tech., India). The absorbance peaks observed in the 3435.34 wave numbers (WN) indicated the presence of strong C-C bonds in the base matrix. Further sharpness in the peaks at the same WN highlighted the formation of strong bonds between CF and the base polymer matrix. Also, the composite samples outlined the peaks corresponding to the presence of the ester group at 2278 WN, carboxyl acid at 1705 WN, and the formation of strong aromatic nitro compounds at 1501WN. The FTIR analysis ascertained that the acceptable bonding characteristics of the 3D-printed hybrid composite structure may be used for proposed industrial applications.

3.7 DMA

Figure 12 shows the dynamic mechanical properties of the 3D-printed ABS-CF structures. In the engineering applications, the materials having storage modulus are greater than the loss modulus are preferred. The value of storage modulus and loss modulus significantly define the materials properties that how materials will break after force is applied. Observed value of the storage modulus has been suggested that increasing the number of in between CF layers increased the storage modulus. The observed value shows the increasing the CF layers have led to increased energy storage capability. This means, the proposed composites having sandwiched CF layers may have good resistance upon crash loading. The similar observations have been noted with the case of loss modulus in which increasing the number of CF layers, the storage modulus becomes increased. In fact, the trend shows that CF sandwiched material combination can also release more energy as compared to ABS. The value of the tan delta has been suggested that increasing the CF layers has increased the starting temperature of thermal degradation but reduced the energy dissipation (vibration damping) properties. The sandwiching of CF in ABS has increased the storage and loss modulus which is a good sign for composites to be applied in crash loading environment, but the use may be limited where high vibration damping required.

4. Conclusions

The investigations performed on the mechanical properties of the 3D-printed hybrid composite structure of ABS and CF highlighted that the mechanical strength of the base matrix increased with an increase in the number of CF layers. The parametric optimization of printing parameters outlined that the acceptable orientation angle of CF in the ABS matrix is 0°. Along with 03 numbers of CF layers and 250 °C printing nozzle temperature, functional parts with acceptable mechanical properties may be fabricated. The morphological analysis (based on SEM–EDS spectroscopy) of hybrid composite structures outlined that the mechanical strength of CF significantly improved the tensile strength, modulus of toughness, and young's modulus of base matrix. Due to an increase in tensile strength, good amorphous, crystalline phases and bonding characteristics have been observed in hybrid ABS-CF composites (based on XRD and FTIR analysis) for the

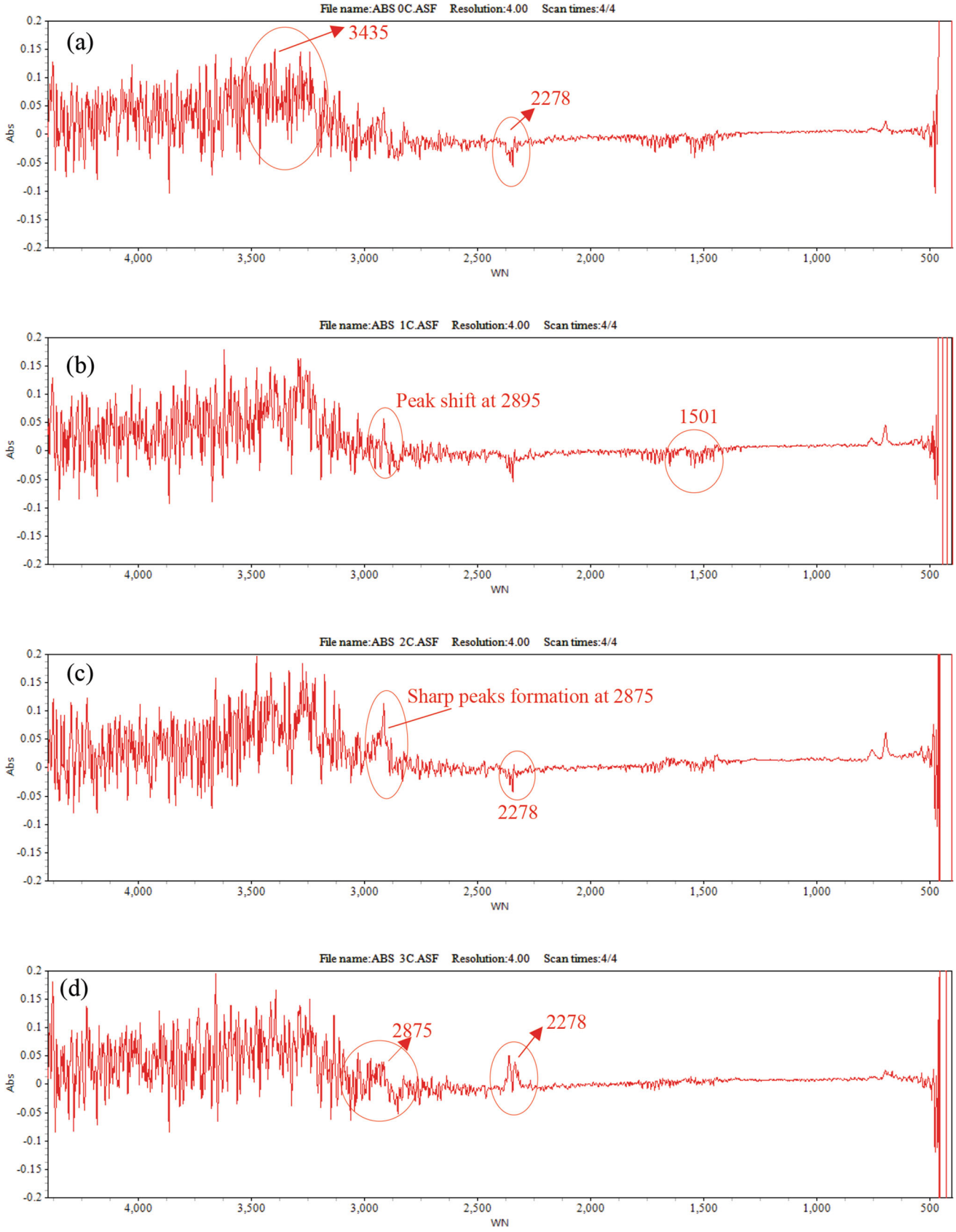

Fig. 11 FTIR results for (a) ABS (2) ABS + 1 CF layer (c) ABS + 2 CF layers (d) ABS + 3 CF layers

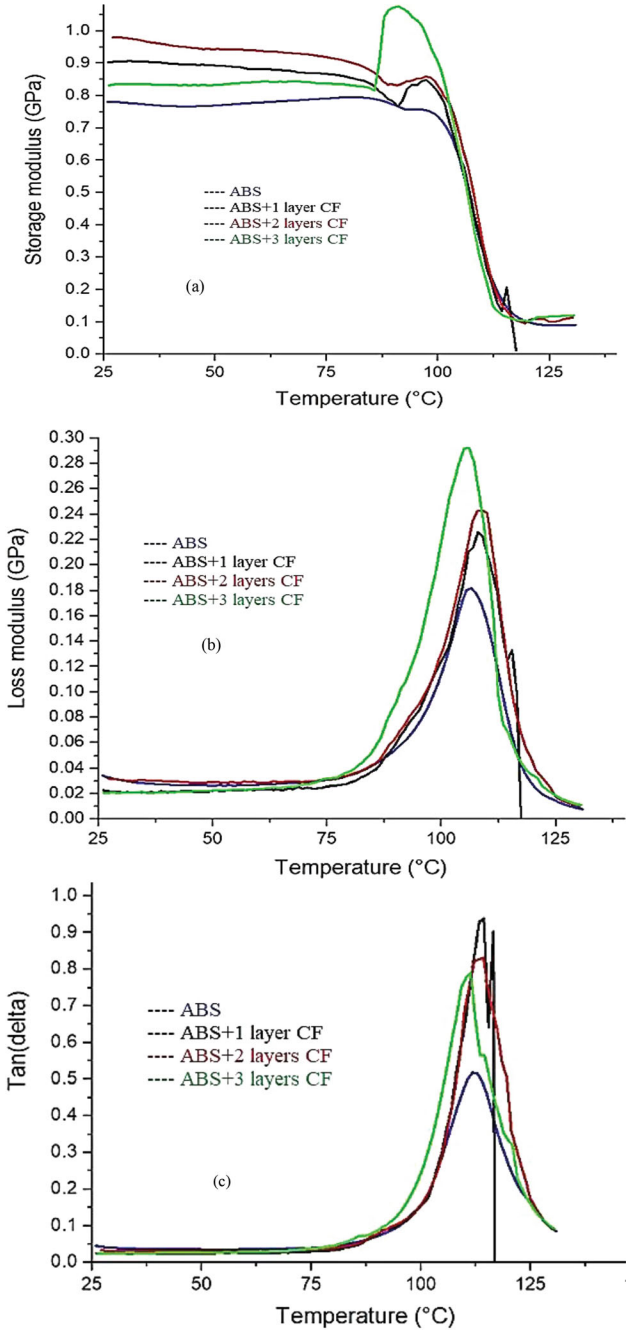

Fig. 12 Plots for (a) storage modulus, (b) loss modulus, and (c) tan delta

proposed advanced engineering applications. The sandwiching of CF in ABS has increased the storage and loss modulus which is a good sign for composites to be applied in crash loading environment, but the use may be limited where high vibration damping required.

Acknowledgments

The authors are thankful to University Centre for Research and Development (UCRD), CU Chandigarh and Manufacturing Research Lab (MRL), and GNDEC Ludhiana for providing the lab facilities throughout this work.

References

1. M.M. Harussani, S.M. Sapuan, G. Nadeem, T. Rafin, and W. Kirubaanand, Recent Applications of Carbon-Based Composites in Defence Industry—A Review, *Def. Technol.*, 2022 https://doi.org/10.1016/j.dt.2022.03.006
2. K. Sugiyama, R. Matsuzaki, M. Ueda, A. Todoroki, and Y. Hirano, 3D Printing of Composite Sandwich Structures Using Continuous Carbon Fibre and Fibre Tension, *Compos. Part A Appl. Sci. Manuf.*, 2018, **113**, p 114–121. https://doi.org/10.1016/j.compositesa.2018.07.029
3. G. Singh and P.M. Pandey, Design and Analysis of Long-Stepped Horn for Ultrasonic-Assisted Sintering, *Adv. Mater. Process. Technol.*, 2021, **7**(2), p 216–226. https://doi.org/10.1080/2374068X.2020.1758604
4. A. Singla and G. Singh, Real-Time Swing-Up and Stabilization Control of a Cart-Pendulum System with Constrained Cart Movement, *Int. J. Nonlinear Sci. Numer.Simul.*, 2017, **18**(6), p 525–539. https://doi.org/10.1515/ijnsns-2017-0040
5. T. Li and L. Wang, Bending Behavior of Sandwich Composite Structures with Tunable 3D-Printed Core Materials, *Compos. Struct.*, 2017, **175**, p 46–57. https://doi.org/10.1016/j.compstruct.2017.05.001
6. N. Singh and G. Singh, Advances in Polymers for Bio-Additive Manufacturing: A State of Art Review, *J. Manuf. Process.*, 2021, **72**, p 439–457. https://doi.org/10.1016/j.jmapro.2021.10.045
7. J. Singh, G. Singh, and P.M. Pandey, Multi-Objective Optimization of Solvent Cast 3D Printing Process Parameters for Fabrication of Biodegradable Composite Stents, *Int. J. Adv. Manuf. Technol.*, 2021, **115**(11–12), p 3945–3964. https://doi.org/10.1007/s00170-021-07423-6
8. S. Singh, G. Singh, C. Prakash, and S. Ramakrishna, Current Status and Future Directions of Fused Filament Fabrication, *J. Manuf. Processes*, 2020, **55**, p 288–306. https://doi.org/10.1016/j.jmapro.2020.04.049
9. S. Singh, G. Singh, C. Prakash, and R. Kumar, On the Mechanical Characteristics of Friction Stir Welded Dissimilar Polymers: Statistical Analysis of the Processing Parameters and Morphological Investigations of the Weld Joint, *J. Braz. Soc. Mech. Sci. Eng.*, 2020 https://doi.org/10.1007/s40430-020-2227-4
10. A. Pandey, G. Singh, S. Singh, K. Jha, and C. Prakash, 3D Printed Biodegradable Functional Temperature-Stimuli Shape Memory Polymer for Customized Scaffoldings, *J. Mech. Behav. Biomed. Mater.*, 2020 https://doi.org/10.1016/j.jmbbm.2020.103781
11. G. Singh, S. Singh, C. Prakash, R. Kumar, R. Kumar, and S. Ramakrishna, Characterization of Three-Dimensional Printed Thermal-Stimulus Polylactic Acid-Hydroxyapatite-Based Shape Memory Scaffolds, *Polym. Compos.*, 2020, **41**(9), p 3871–3891. https://doi.org/10.1002/pc.25683
12. R. Kumar et al., On Mechanical, Physical, and Bioactivity Characteristics of Material Extrusion Printed Polyether Ether Ketone, *J. Mater. Eng. Perform.*, 2022 https://doi.org/10.1007/s11665-022-07519-4
13. J. Naranjo-Lozada, H. Ahuett-Garza, P. Orta-Castañón, W.M.H. Verbeeten, and D. Sáiz-González, Tensile Properties and Failure Behavior of Chopped and Continuous Carbon Fibre Composites Produced by Additive Manufacturing, *Addit. Manuf.*, 2019, **26**(December 2018), p 227–241. https://doi.org/10.1016/j.addma.2018.12.020
14. F. Ning, W. Cong, Y. Hu, and H. Wang, Additive Manufacturing of Carbon Fibre-Reinforced Plastic Composites Using Fused Deposition Modeling: Effects of Process Parameters on Tensile Properties, *J. Compos. Mater.*, 2017, **51**(4), p 451–462.
15. W. Zhong, F. Li, Z. Zhang, L. Song, and Z. Li, Short Fibre Reinforced Composites for Fused Deposition Modeling, *Mater. Sci. Eng., A*, 2001, **301**(2), p 125–130.
16. F. Van Der Klift et al., 3D Printing of Continuous CF Reinforced Thermo-Plastic (CFRTP) Tensile Test Specimens, *Open J. Compos. Mater.*, 2016, **6**(01), p 18.
17. L.G. Blok, M.L. Longana, H. Yu, and B.K.S. Woods, An Investigation Into 3D Printing of Fibre Reinforced Thermoplastic Composites, *Addit. Manuf.*, 2018, **22**(November 2017), p 176–186. https://doi.org/10.1016/j.addma.2018.04.039
18. A. Das et al., Rheological Investigation of Nylon-Carbon Fiber Composites Fabricated using Material Extrusion-Based Additive Manufacturing, *Polym. Compos.*, 2021, **42.11**, p 6010–6024.
19. N. Mosleh, A.M. Rezadoust, and S. Dariushi, Determining Process-Window for Manufacturing of Continuous Carbon Fiber-Reinforced

Composite Using 3D-Printing, *Mater. Manuf. Processes*, 2021, **36**(4), p 409–418.
20. A. Galatas et al., Additive Manufactured Sandwich Composite/ABS Parts for Unmanned Aerial Vehicle Applications, *Polymers*, 2018, **10.11**, p 1262.
21. Z. Wang et al., Mechanical and Self-Monitoring Behaviors of 3D Printing Smart Continuous Carbon Fiber-Thermoplastic Lattice Truss Sandwich Structure, *Compos. Part B: Eng.*, 2019, **176**, p 107215.
22. C. Yang, X. Tian, T. Liu, Y. Cao, and D. Li, 3D Printing for Continuous Fiber Reinforced Thermoplastic Composites: Mechanism and Performance, *Rapid Prototyp. J.*, 2017, **23**(1), p 209–215.
23. H. Zhang, J. Chen, and D. Yang, Fibre Misalignment and Breakage in 3D Printing of Continuous Carbon Fibre Reinforced Thermoplastic Composites, *Addit. Manuf.*, 2021, **38**, p 101775.
24. A. Todoroki et al., Tensile Property Evaluations of 3D Printed Continuous Carbon Fiber Reinforced Thermoplastic Composites, *Adv. Compos. Mater.*, 2020, **292**, p 147–162.
25. K. Dong, L. Liu, X. Huang, and X. Xiao, 3D Printing of Continuous Fibre Reinforced Diamond Cellular Structural Composites and Tensile Properties, *Compos. Struct.*, 2020, **250**(April), p 112610. https://doi.org/10.1016/j.compstruct.2020.112610
26. D. Lasikun, E. Ariawan, Surojo, and J. Triyono, "Effect of Fibre Orientation on Tensile and Impact Properties of Zalacca Midrib Fibre-HDPE Composites by Compression Molding. In: AIP Conf. Proc., vol. 1931, no. February, 2018, doi: https://doi.org/10.1063/1.5024119
27. M.M. Maraş, Mechanical and Fracture Behavior of Geopolymer Composites Reinforced with Fibres by Using Nano - TiO_2, *J. Braz. Soc. Mech. Sci. Eng.*, 2021, **43**(9), p 1–18. https://doi.org/10.1007/s40430-021-03135-w
28. S. Mortazavian and A. Fatemi, Effects of Fibre Orientation and Anisotropy on Tensile Strength and Elastic Modulus of Short Fibre Reinforced Polymer Composites Composites Part B: Engineering, *Compos. B*, 2014 https://doi.org/10.1016/j.compositesb.2014.11.041
29. A. Balaji et al., Study on Mechanical and Morphological Properties of Sisal/banana/coir Fibre-Reinforced Hybrid Polymer Composites, *J. Braz. Soc. Mech. Sci. Eng.*, 2019, **41**(9), p 1–10. https://doi.org/10.1007/s40430-019-1881-x
30. D.D. Phan, Z.R. Swain, and M.E. Mackay, Rheological and Heat Transfer Effects in Fused Filament Fabrication, *J. Rheol.*, 2018, **62**(5), p 1097–1107.
31. M.E. Mackay, The Importance of Rheological Behavior in the Additive Manufacturing Technique Material Extrusion, *J. Rheol.*, 2018, **62**(6), p 1549–1561.
32. A. Das, E.L. Gilmer, S. Biria, and M.J. Bortner, Importance of Polymer Rheology on Material Extrusion Additive Manufacturing: Correlating Process Physics to Print Properties, *ACS Appl. Polym. Mater.*, 2021, **3**(3), p 1218–1249.